SAND2018-9734J

pH-Dependent Assembly of Porphyrin-Silica Nanocomposites and their Application in Targeted Photodynamic Therapy

Jiefei Wang,[1] Yong Zhong,[1] Xiao Wang,[1] Weitao Yang,[2] Feng Bai,[1, 3,]* Bingbo Zhang,[2,]* Leanne Alarid,[5] Kaifu Bian,[5] and Hongyou Fan[4, 5,]*

[1]Key Laboratory for Special Functional Materials of the Ministry of Education, Henan University, Kaifeng 475004, P. R. China

[2]Institute of Photomedicine, Shanghai Skin Disease Hospital, The Institute for Biomedical Engineering & Nano Science, Tongji University School of Medicine, Shanghai 200443, China

[3]Collaborative Innovation Center of Nano Functional Materials and Applications, Henan University, Kaifeng 475004, China

[4]Department of Chemical and Biological Engineering, Albuquerque, University of New Mexico, Albuquerque, New Mexico 87106, USA

[5]Sandia National Laboratories, Albuquerque, New Mexico 87185, USA

Corresponding author emails, phone numbers, and fax numbers:

H.F. (hfan@sandia.gov), Tel: (505) 272-7128, Fax: (505) 272-7336

F.B. (baifengsun@126.com), Tel: 86-15039024866, Fax: 86-0371-23883868

B.Z. (bingbozhang@tongji.edu.cn), Tel: 86-13817752609, Fax: 86-021-65987071

ABSTRACT

Structurally controlled nanoparticles, such as core-shell nanocomposite particles by combining two or more compositions possess enhanced or new functionalities that benefited from synergistic coupling of the two components. Here we report new nanocomposite particles with self-assembled porphyrin arrays as the core surrounded by amorphous silica as the shell. Synthesis of such nanocomposite nanoparticles was conducted through a combined surfactant micelle confined self-assembly and silicate sol-gel process using optically active porphyrin as a functional building block. Depending on kinetic conditions, these particles exhibit structure and function at multiple length scales and locations. At the molecular scale, the porphyrins as the building blocks provide well defined macromolecular structure for non-covalent self-assembly and unique chemistry for high-yield generation of singlet oxygen for photodynamic therapy (PDT). On the nanoscale, controlled non-covalent interactions of the porphyrin building block result in extensive self-assembled porphyrin network that enables efficient energy transfer and impressive fluorescence for cell labeling, evidenced by absorption and photoluminescence spectra. Finally, the thin silicate shell on the nanoparticle surface allows easy functionalization, and the resultant targeting porphyrin-silica nanocomposites can selectively destroy tumor cells upon receiving light irradiation.

KEYWORDS: Self-assembly, photosensitizer, porphyrins, photodynamic therapy, singlet oxygen.

Active nanoparticles are an important class of nanomaterials that exhibit important applications in nanoelectronics, catalysis, and phototherapy[1-5]. Besides their unique size and shape dependent physical properties, structurally controlled nanoparticles, such as core-shell composite nanoparticles by combining two or more compositions, possess enhanced or new functionalities that resulted from synergistic coupling of the two components. Ability to tune composition, structure, and dimension of nanoparticles has stimulated considerable efforts to develop methods to prepare nanocomposite particles. Porphyrins, similar to many biomacromolecules such as chlorophyll, have well-defined structure and surface chemistry. They are vital pigments in some biological energy transduction processes including light harvesting, photo-catalytic synthesis and therapy, water splitting in plants, algae, and bacteria [6]. Inspired by their utility and function, recently, there has been a widespread interest in the preparation of porphyrin nanoparticles and their ordered arrays through self-assembly of molecular building blocks, aiming to emulate natural light harvesting processes and energy storage and to develop new nanostructured materials[7, 8]. It is shown that efficient electron or energy transport relies on not only the intermolecular forces (e.g., hydrogen bonding, π-π stacking, etc), but also the long range ordering of intermolecular arrangements, morphology, and dimension control. For example, formation of ordered porphyrin nanoparticles with control spatial or axial porphyrin arrangement leads to significantly better photo-catalytic activity[9, 10]. Thus, the potential of these materials is directly connected to the ability of controlling and engineering of well-defined material structures including size, shape, dimension, and spatial or axial intermolecular arrangements,

which drives extensive synthetic efforts. Earlier works on the formation of porphyrin arrays are limited to 2-dimensional (D) arrays with ill-defined material morphology and lack of long range ordered network for efficient electron or energy transport[11, 12]. 3-D porphyrin assemblies have been demonstrated to improve transport through solid-state synthesis [13]. The resulting materials exhibit uncontrolled external morphology and structure dimension, which limits their efficiency of energy transfer. More importantly, ability to engineer the assembly of porphyrins to be biocompatible is of great importance for bioimaging and phototherapy applications. To the end, synthesis of porphyrin-silica composite particles through sol-gel routes has been demonstrated to provide both biofunctionalization through silica layer and photosensitizers for PDT[14, 15, 16]. However, in these cases, the porphyrins were randomly entrapped inside the silica particles lack of long range ordering, which is not ideal for electron and/or energy transport.

Here we developed a new method to synthesize self-assembled porphyrin-silica nanocomposite particles with ordered porphyrin network as the core surrounded by amorphous silica as the shell. The long range ordering of porphyrin network enables efficient energy transfer and impressive fluorescence for cell labeling while the silica layer provides opportunity for biofunctionalization. The synthesis of these particles was conducted through combined surfactant assisted cooperative self-assembly and sol-gel process using silicate precursors and photoactive precursor zinc-tetra (4-pyridyl) porphyrin (ZnTPP) as a building block. Through confined non-covalent interactions of ZnTPP within surfactant micelles, different porphyrin-silica

nanocomposite particles including core-shell particles ($ZnTPP@SiO_2$) and solid particles ($ZnTPP\text{-}SiO_2$) were synthesized. For the core-shell structured particles, the resulted nanoparticles consist of ordered porphyrin arrays in the center core that is surrounded by a thin layer of silica. These nanoparticles exhibit enhanced optical properties versus individual porphyrin monomers due to collective behaviors resulted from their ordered self-assemblies. For the solid, namely, the $ZnTPP\text{-}SiO_2$ particles, the particles consist of mesophase of self-assembled ZnTPP oligomer clusters/silica. The overall preparation is illustrated in **Scheme 1**. ZnTPP was first dissolved in an acidic solution through a protonation process to form $ZnTPP\text{-}H_4^{4+}$.[17,18] The self-assembly of ZnTPP arrays was subsequently initiated by combining the $ZnTPP\text{-}H_4^{4+}$ acidic aqueous solution

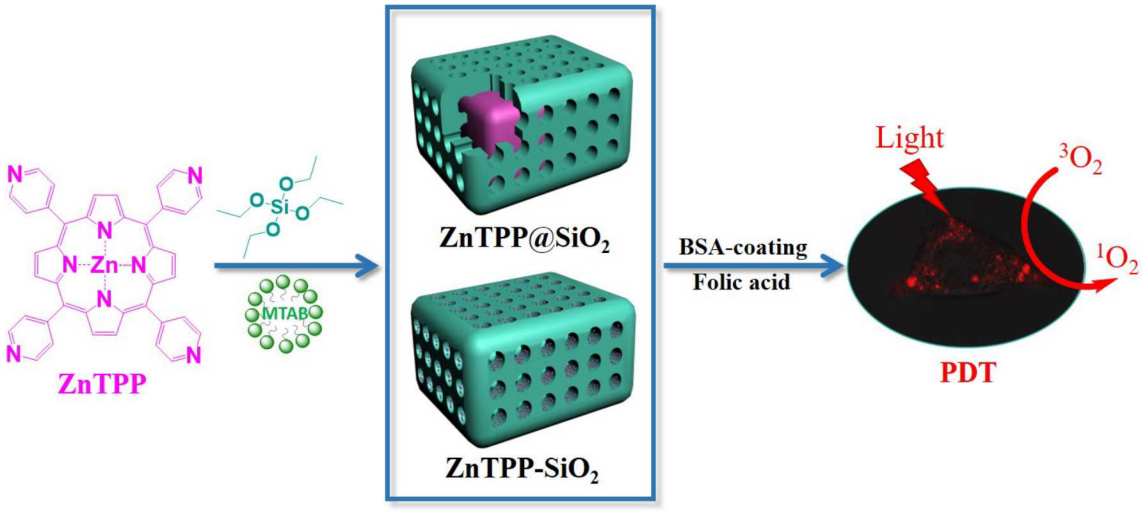

Scheme 1. Schematic diagram for controlled formation of core-shell structured $ZnTPP@SiO_2$ and solid $ZnTPP\text{-}SiO_2$ nanocomposite particles.

with a basic surfactant solution under vigorous stirring (see Materials and Methods in Supporting Information). Finally 300 μL of tetraethyl orthosilicate (TEOS) in methanol (20% v/v) was added into the above solution with 20 μL each time and 15 min interval to initiate the silicate hydrolysis and condensation. The mixture was stirred for 48 hours at room temperature. The final nanoparticle products were collected by centrifugation and washed with water twice to remove byproducts and the free surfactants.

The porphyrin-silica nanocomposite particles displayed high monodispersity and well-defined morphologies as shown in the transmission electron microscopy (TEM) images (Figure 1, A and C). Particle size distribution statistics of the particles indicated that these nanocomposite particles have an average diameter of 89.5 nm for the core-shell particles and 80.0 nm for the solid particles (see Figure S1). High resolution TEM images (Figure 1, B and D) revealed more detailed structural information of the particles. Crystalline lattice fringes can be clearly seen inside the core-shell particles. These lattice fringes are resultant from the self-assembled ZnTPP arrays. More detailed pH-dependent inner structures (see Figure S2) indicated a structural transition from core-shell to solid inner structures. The addition of the acidic ZnTPP-H_4^{4+} solution into the base solution results in an acid-base neutralization reaction. The acid-base neutralization deprotonates the tetrapyridinium cations, producing insoluble ZnTPPs that are thus encapsulated within the core of hydrophobic micelles similar to what occurs with surfactant encapsulation of hydrophobic nanoparticles or oil-like species into micelles [19]. Subsequent self-assembly driven by intermolecular axial coordination (Zn-N) and non-covalent interactions such

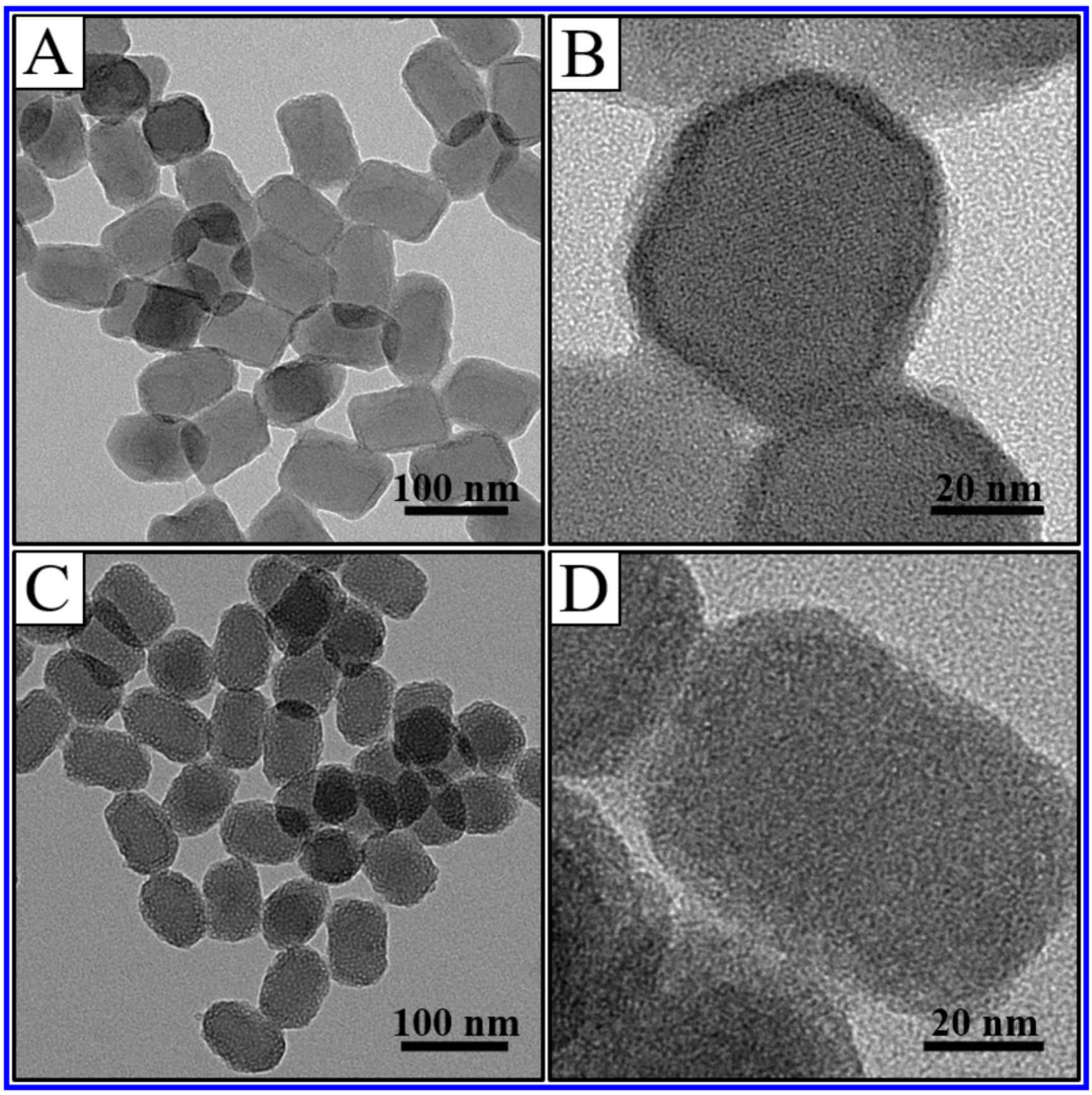

Figure 1. TEM images of porphyrin-silica nanocomposite particles. (A) and (B) Core-shell structured nanoparticles (ZnTPP@SiO_2). (C) and (D) Solid particles (ZnTPP-SiO_2).

as hydrophobic-hydrophobic interactions and aromatic π-π stacking between molecules or surfactants initiates nucleation and growth of ordered J-aggregate ZnTPP arrays [18, 20, 21]. X-ray diffraction (XRD) patterns (see Figure S3) indicated the crystal structure consists of mixture of

tetragonal and hexagonal phases from self-assembled porphyrin arrays[17, 20]. Surrounding the ordered porphyrin lattices, a thin layer of amorphous silica with a thickness of ~5 nm can be clearly observed. Different from the core-shell particles, the ZnTPP-SiO_2 solid particles were observed to be amorphous from the TEM images (Figure 1, C and D). XRD patterns of these particles (see Figure S3) show a major amorphous phase with some small weak peaks that belong to the tetragonal phase. TEM images in Figure 1 also indicated formation of worm like mesophase that is uniformly distributed within the particles.

Optical spectroscopy studies provided clear insight of the porphyrin self-assembly process. The porphyrin-silica particles showed characteristic absorption spectra from the porphyrin chromophore with a Soret band from 400 nm to 460 nm and Q-band between 500 nm and 650 nm (Figure 2). The intense and sharp Soret band (B-band) of the ZnTPP monomer (at ~424 nm) becomes split upon self-assembly with a red-shifted band arising at ~450 nm, which confirms formation of J-aggregation. In addition, all the new bands cover a broader region of the spectrum. Along with the decrease of solution pH, the optical band becomes much broader and farther red shift, which indicates extensive electron delocalization due to the conjugated porphyrin networks from the extensive porphyrin self-assembly. The Q-bands are relatively

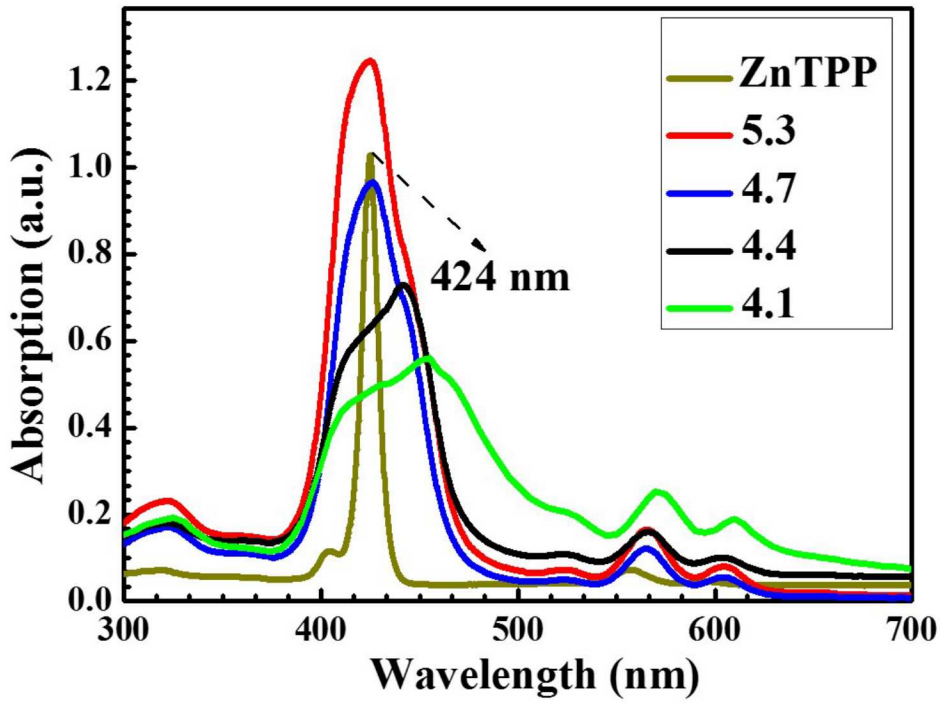

Figure 2. UV-Vis absorption spectra of ZnTPP monomer and ZnTPP-silica nanocomposite particles synthesized at different pH.

enhanced in intensity when the solution pH decreases. This is advantageous for exciton transport since it is the exciton coupling between these states that are relevant for exciton transport [22].

Detailed experimental studies suggest that the self-assembly process is critically influenced by the solution pH. At low pH, acidic conditions cause slow hydrolysis of TEOS [23], but confined self-assembly of porphyrin proceed extensively according to UV-vis results (Figure 2). At this condition, silica tends to form linear molecules that are occasionally cross-linked [23]. The combined results are the fast formation of self-assembled porphyrin particles as the core

surrounded by condensed silica as the shell layer. These molecular chains entangle and form additional branches resulting in gelation and formation of ZnTPP@SiO_2 core-shell particles. At relatively high pH, hydrolysis and condensation of TEOS is relatively faster [23] and porphyrin self-assembly is relatively slow based on UV-vis results (Figure 2). More highly branched silica clusters that are not interpenetrable, formed before drying and thus behave as discrete species. Gelation occurs by linking of the clusters with self-assembled porphyrin oligomers, which leads to mesophase of self-assembled ZnTPP oligomer clusters and silica. Thermal gravimetric analysis (TGA) (see Figure S4) of these nanocomposite particles revealed that there are more porphyrins in the core-shell particles than in the solid particles.

Singlet oxygen measurements by ESR on the resulted nanocomposite particles revealed high yields of singlet oxygen (Figure 3) upon light irradiation[24, 25]. ZnTPP@SiO_2 nanocomposite particles with J-aggregated ZnTPP prepared at pH 4.1 displayed double enhancement of singlet oxygen production compared with that of ZnTPP-SiO_2 nanocomposites synthesized at pH 5.3, which is probably due to the increased porphyrin π-π stacking and out-of-plane coordination of Zn and pyridine. Metal porphyrins are known to facilitate the energy transfer via intersystem coordination crossing, which helps the formation of an out-of-plane structures and generation of more singlet oxygen [26]. The high yields of singlet oxygen are of great importance for PDT applications. To investigate cell uptake and localization of the nanoparticles, we first functionalized the nanocomposite particles with bovine serum albumin (BSA) to enhance their

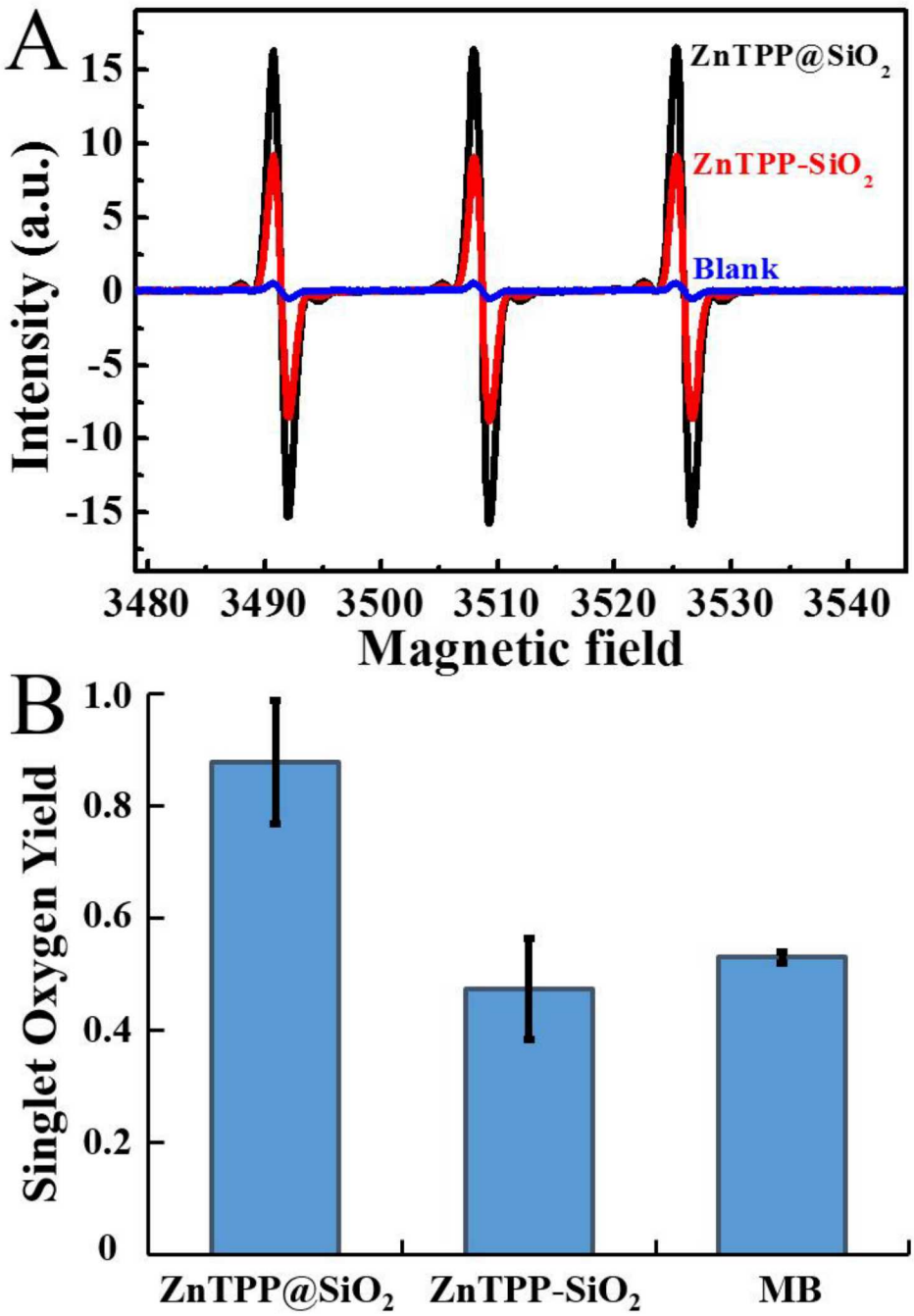

Figure 3. Singlet oxygen detection of core-shell particles and solid particles. (A) ESR results of singlet oxygen detection for different particles (blank sample was the ZnTPP@SiO_2 sample without light irradiation). (B) Yield of singlet oxygen from ZnTPP@SiO_2, ZnTPP-SiO_2, and MB as a reference ($\Phi r = 0.53$). $\Phi_{ZnTPP@SiO2} = 0.87$ and $\Phi_{ZnTPP-SiO2} = 0.49$.

hydrophilicity and followed by folic acid (FA) to improve targeting efficacy to cancer cells [27]. FT-IR measurements (see Figure S5) showed that FA was grafted onto nanoparticles through amide linkage with BSA. After modification, strong absorption peaks around 1650 cm^{-1} attributable to the amide linkage (amide, C=O) appeared in both spectra of FA-ZnTPP@SiO_2 and FA-ZnTPP-SiO_2.

The targeting capability of FA-labeled ZnTPP@SiO_2 and ZnTPP-SiO_2 was evaluated on HeLa cancer cells with overexpressed folate receptors on their cell surfaces. Confocal microscopic imaging showed that FA functionalization obviously facilitates cellular uptake of nanocomposite particles by HeLa cells in comparison with those particles without FA functionalization. HeLa cells were incubated with 8 μM of these two kinds of nanocomposite particles for 2 hours at 37 ℃, respectively. The corresponding cell images were collected and showed in Figure 4. It clearly showed that the nanocomposite particles without FA moieties mainly attached around the cell membranes via physical absorption, while FA-labeled nanocomposite particles largely located in the cytolymph. This difference in cellular location is mainly attributed to the FA-mediated endocytosis effect that facilitates the particles entering into the cells.

The dose-dependent cell uptake of FA-ZnTPP@SiO_2 and FA-ZnTPP-SiO_2 was further performed in HeLa cells. HeLa cells were incubated with these nanocomposite particles at

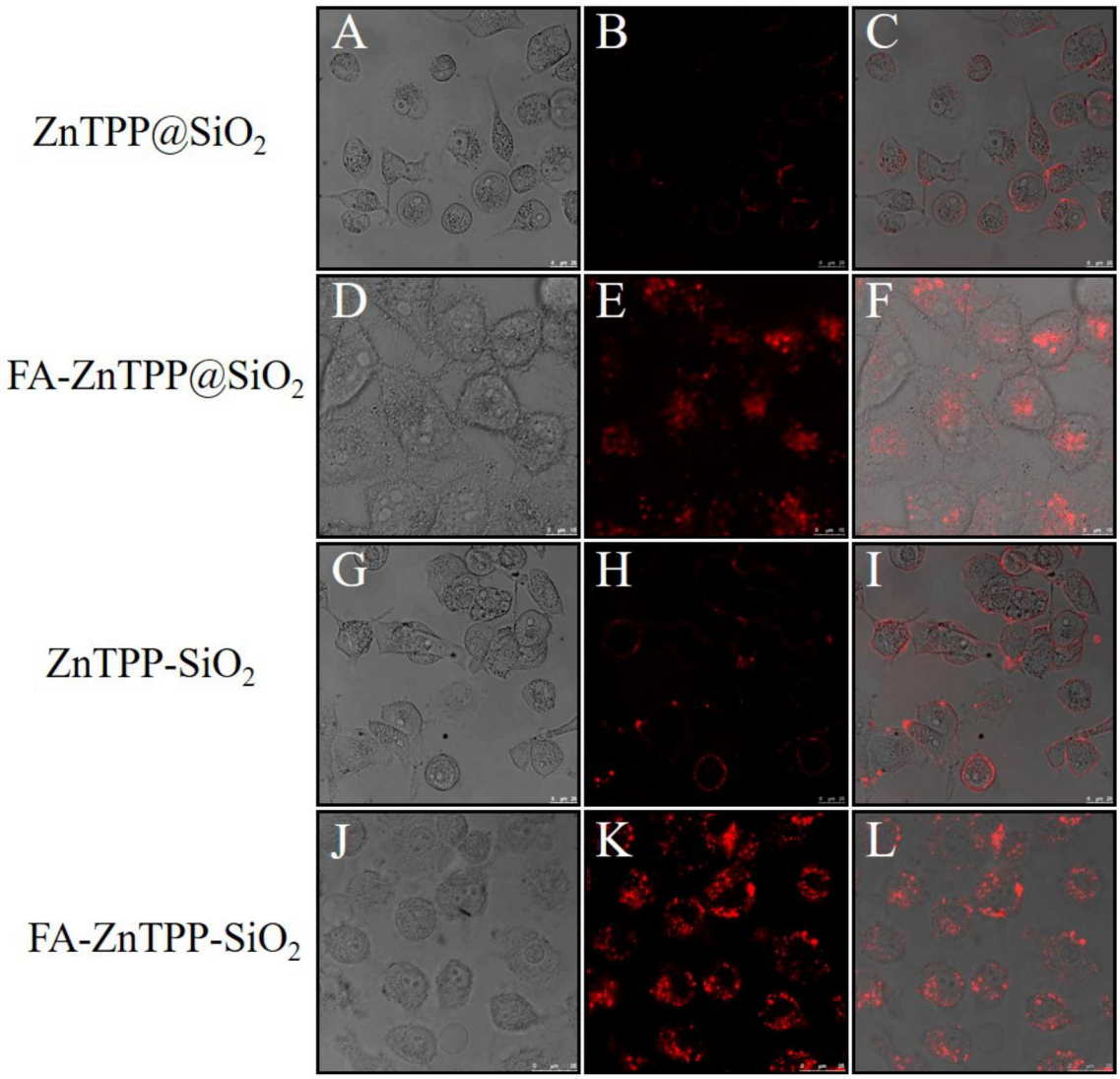

Figure 4. Confocal microscopy images of HeLa cells incubated with 8 μM of core-shell and solid nanocomposite particles, respectively. (A-C) ZnTPP@SiO_2. (D-F) FA-ZnTPP@SiO_2, (G-I) ZnTPP-SiO_2, (J-L) FA-ZnTPP-SiO_2. Imaging conditions: bright field images in the first column, fluorescence images in the second column, and merged images of the combined bright field images and fluorescence images in the third column.

varying concentrations of 2 μM, 4 μM and 8 μM respectively. The results shown in confocal microscopy images (see Figure S6) showed increased fluorescence intensity corresponding to the increased concentrations of nanocomposite particles, which suggests higher dose can pressurize more endocytosis of photosensitizers. Flow cytometric analysis further quantitatively presented a gradually increased intracellular fluorescence from 2 μM to 8 μM (see Figure S7). It should be noted that the cell uptake profiles of ZnTPP@SiO_2 and ZnTPP-SiO_2 were found similar, regardless of FA labeling or not in HeLa cells. The above results collectively showed that FA modification can significantly enhance the endocytosis of nanocomposite particles in HeLa cells, and particularly this endocytosis was positively related to the dose of the nanocomposite particles.

The PDT efficacy of the core-shell and solid particles was studied on HeLa cells. By incubating the nanocomposite particles with HeLa cells at different concentrations for 2 hours, as shown in Figure 5, the cell viabilities in the groups of FA-ZnTPP@SiO_2 and FA-ZnTPP-SiO_2 were both found significantly decreased along with the increase of the irradiation time upon exposure to a 635 nm laser light with a relatively low density of 100 mW/cm^2. Moreover, the nanocomposite particle–mediated cell killing was found to be dose-dependent, showing that bigger doses exert higher killing efficacy. It should be noted that the cell viabilities in the control groups without irradiation were close up to 90 %, suggesting good biocompatibility and low dark toxicity of these nanocomposite particles. More importantly, core-shell structured FA-ZnTPP@SiO_2 exhibited higher PDT efficacy than that of solid FA-ZnTPP-SiO_2 particles under

the same experimental conditions. This improved PDT outcome could be attributed to the higher singlet oxygen generation in the core-shell structured ZnTPP@SiO_2 (see Figure 3), although these two structures showed a similar cell uptake pattern in HeLa cells, which is shown in the Figure 4, Figure S6, and Figure S7.

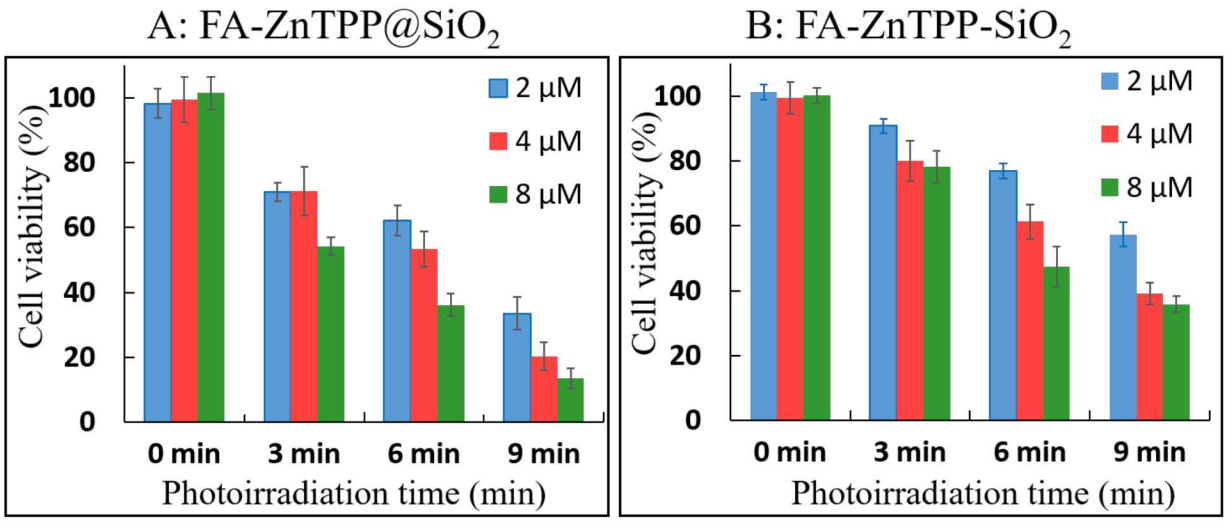

Figure 5. Viability of HeLa cells after treated with composite particles. (A) Core-shell particles and (B) solid particles at different concentrations (2 μM, 4 μM, 8 μM) with a 635 nm laser exposure. The irradiation time was 0 min, 3 min, 6 min, and 9 min for each sample at low density of 100 mW/cm^2.

In conclusion, the combined self-assembly of porphyrin with silicate sol-gel processes provides a new approach to synthesize highly ordered porphyrin-silica nanocomposite particles that enable synergetic functions. The porphyrin self-assembly relies on non-covalent interactions

between amphiphilic surfactants and porphyrin building blocks leading to nucleation and growth of ordered porphyrin arrays with unique structures and functions on multiple length scales. The thin silicate shell allows convenient functionalization to improve biocompatibility for cell uptakes. Without silica layer, the self-assembled porphyrin particles are hydrophobic and not biocompatible to cells. Control of pH conditions in the self-assembly solution is an important factor for tuning the final nanostructures. Low pH conditions promote porphyrin noncovalent self-assembly, forming core-shell particles. However, high pH conditions are favorable for silicate sol-gel process, forming solid porphyrin-silica mesophase particles. The resultant photoactive porphyrin-silica nanocomposite particles were found to be penetrable into the tumor cells, which can be facilitated by FA-mediated endocytosis effect. More importantly, both of the two types of nanocomposites can generate lethal singlet oxygen, but the core-shell structured particles were found to have an even better yield. This structure-dependent and enhanced PDT activity is further demonstrated in the phototherapy with more tumor cells destroyed by the core-shell structured particles.

ASSOCIATED CONTENT

Supporting Information. Preparation of core-shell nanoparticles and their characterizations including TEM, XRD, FTIR, UV-vis, TGA, and confocal microscopy images that are available

free of charge.

AUTHOR INFORMATION

Corresponding Author

H.F. (hfan@sandia.gov); F.B. (baifengsun@126.com); B.Z. (bingbozhang@tongji.edu.cn)

Author Contributions

The manuscript was written through contributions of all authors. All authors have given approval to the final version of the manuscript. HF conceived the idea. JFW, YZ, XW, FB, LA, KB performed the synthesis, structure and optical characterization. WY and BBZ performed biofunctionalization, cell and phototherapy experiments. All authors commented on the manuscript and contributed to the writing of the manuscript.

Note

The authors declare no competing financial interest.

ACKNOWLEDGMENT

This work was supported by the U.S. Department of Energy, Office of Basic Energy Sciences, Division of Materials Sciences and Engineering. F.B. acknowledges the support from the National Natural Science Foundation of China (21422102, 21771055, U1604139, 21171049, 81371618), Plan For Scientific Innovation Talent of Henan Province (No. 174200510019), and

Program for Changjiang Scholars and Innovative Research Team in University (No.PCS IRT_15R18). Sandia National Laboratories is a multimission laboratory managed and operated by National Technology and Engineering Solutions of Sandia, LLC., a wholly owned subsidiary of Honeywell International, Inc., for the U.S. Department of Energy's National Nuclear Security Administration under contract DE-NA0003525.

REFERENCES

(1) Zhang, Q.; Lee, I.; Joo, J. B.; Zaera, F.; Yin, Y. *Acc. Chem. Res.* **2013,** 46, 1816-1824.
(2) Lu, Y.; Yin, Y.; Li, Z.-Y.; Xia, Y. *Nano Lett.* **2002,** 2, 785-788.
(3) Zhang, C.; Chen, B.-Q.; Li, Z.-Y.; Xia, Y.; Chen, Y.-G. *J. Phys. Chem. C* **2015,** 119, 16836-16845.
(4) Ma, Y.; Li, W.; Cho, E. C.; Li, Z.; Yu, T.; Zeng, J.; Xie, Z.; Xia, Y. *ACS Nano* **2010,** 4, 6725-6734.
(5) Ghosh Chaudhuri, R.; Paria, S. *Chem. Rev.* **2012,** 112, 2373-2433.
(6) Zuber, H. a. C., R. J. , Structure and organization of purple bacterial antenna complexes. In *Anoxygenic Photosynthetic Bacteria*, R. E. Blankenship, M. T. M. a. C. E. B., Ed. Kluwer Acad. Publ., The Netherlands, 1995: pp pp. 315-348.
(7) Dolphin, D., *The Porphyrins*. Academic Press: New York, 1978; Vol. 3.
(8) Drain, C. M.; Chen, X.; Nalwa, H. S., *Encyclopedia of Nanoscience & Nanotechnology*. 2004: 593.
(9) Bai, F.; Sun, Z.; Wu, H.; Haddad, R. E.; Xiao, X.; Fan, H. *Nano Lett.* **2011,** 11, 3759-3762.
(10) Wang, J.; Zhong, Y.; Wang, L.; Zhang, N.; Cao, R.; Bian, K.; Alarid, L.; Haddad, R. E.; Bai, F.; Fan, H. *Nano Lett.* **2016,** 16, 6523-6528.
(11) Barlow, D. E.; Scudiero, L.; Hipps, K. W. *Langmuir* **2004,** 20, 4413-4421.
(12) Scudiero, L.; Hipps, K. W.; Barlow, D. E. *J. Phys. Chem. B* **2003,** 107, 2903-2909.
(13) Goldberg, I. *Chem. Commun.* **2005**, 1243-1254.
(14) Xing, C.; Xu, Q.; Tang, H.; Liu, L.; Wang, S. *J. Am. Chem. Soc.* **2009,** 131, 13117-13124.
(15) Papacídero, A. T.; Rocha, L. A.; Caetano, B. L.; Molina, E.; Sacco, H. C.; Nassar, E. J.; Martinelli, Y.; Mello, C.; Nakagaki, S.; Ciuffi, K. *J. Colloids Surf., A* **2006,** 275, 27-35.

(16) Bechet, D.; Couleaud, P.; Frochot, C.; Viriot, M.-L.; Guillemin, F.; Barberi-Heyob, M. *Trends Biotechnol*. **2008,** 26, 612-621.
(17) Bai, F.; Sun, Z.; Wu, H.; Haddad, R. E.; Coker, E. N.; Huang, J. Y.; Rodriguez, M. A.; Fan, H. *Nano Lett*. **2011,** 11, 5196-5200.
(18) Bai, F.; Wu, H.; Haddad, R. E.; Sun, Z.; Schmitt, S. K.; Skocypec, V. R.; Fan, H. *Chem. Commun*. 46, 4941-4943.
(19) Fan, H.; Yang, K.; Boye, D. M.; Sigmon, T.; Malloy, K. J.; Xu, H.; López, G. P.; Brinker, C. J. *Science* **2004,** 304, 567-571.
(20) Zhong, Y.; Wang, J.; Zhang, R.; Wei, W.; Wang, H.; Lü, X.; Bai, F.; Wu, H.; Haddad, R.; Fan, H. *Nano Lett*. **2014,** 14, 7175-7179.
(21) Zhong, Y.; Wang, Z.; Zhang, R.; Bai, F.; Wu, H.; Haddad, R.; Fan, H. *ACS Nano* **2014,** 8, 827-833.
(22) Martin, K. E.; Wang, Z.; Busani, T.; Garcia, R. M.; Chen, Z.; Jiang, Y.; Song, Y.; Jacobsen, J. L.; Vu, T. T.; Schore, N. E.; Swartzentruber, B. S.; Medforth, C. J.; Shelnutt, J. A. *J. Am. Chem. Soc*. **2010,** 132, 8194-8201.
(23) Brinker, C. J.; Sherer, G. W., *So-Gel Science: the Physics and Chemistry of Sol-Gel Processing*. Academic Press: London, 1990.
(24) Dougherty, T. J. *J. Photochem. Photobiol*. **1987,** 45, 879-889.
(25) Cheng, S.-H.; Lee, C.-H.; Yang, C.-S.; Tseng, F.-G.; Mou, C.-Y.; Lo, L.-W. *J. Mater. Chem*. **2009,** 19, 1252-1257.
(26) Zhao, Q.; Wang, Y.; Xu, Y.; Yan, Y.; Huang, J. *Sci. Rep*. **2016,** 6, 31339.
(27) Huang, P.; Xu, C.; Lin, J.; Wang, C.; Wang, X.; Zhang, C.; Zhou, X.; Guo, S.; Cui, D. *Theranostics* **2011,** 1, 240-250.

for TOC only

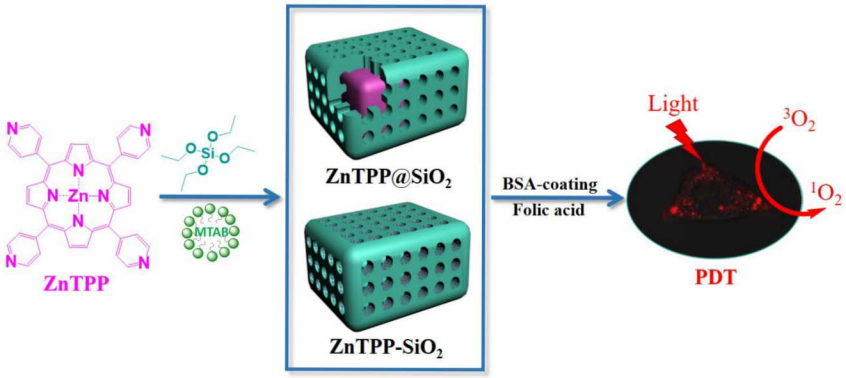
ZnTPP
Si
MTAB
ZnTPP@SiO2
ZnTPP-SiO2
BSA-coating
Folic acid
Light
3O2
1O2
PDT